Determination of Peptide Amide Configuration in a Model Amyloid Fibril by Solid-State NMR

P. R. Costa,[†,‡] D. A. Kocisko,[‡,§] B. Q. Sun,[†,‡,∥] P. T. Lansbury, Jr.,[⊥] and R. G. Griffin*[,†,‡]

Contribution from the Francis Bitter Magnet Laboratory and Department of Chemistry, Massachusetts Institute of Technology, Cambridge, Massachusetts 02139, and the Center for Neurologic Diseases, Brigham and Women's Hospital and Harvard Medical School, Boston, Massachusetts 02115

Received May 8, 1997. Revised Manuscript Received July 8, 1997[⊗]

Abstract: The β-amyloid proteins (Aβ), especially the variant Aβ1−42, are the primary constituent of the amyloid plaques which are characteristic of Alzheimer's disease (AD). The C-terminus of Aβ has been identified as crucial for rapid amyloid formation. A 9-residue C-terminal fragment of Aβ (designated β34−42, with sequence LMVGGVVIA) forms a structured aggregate which is classified as an amyloid fibril based primarily on its morphological and solubility properties and the classic cross-β fiber diffraction pattern it displays. We have adopted this aggregate as a model of the Aβ-dominated amyloid plaques associated with AD. Previous results from a series of internuclear ^{13}C−^{13}C distance measurements along the peptide backbone indicate that the β34−42 backbone conformation differs considerably from that of the classic β-sheet, possibly including an unusual *cis* amide bond in the peptide's central glycyl−glycyl region. Here we report evidence which demonstrates the presence of a *trans* configuration at the peptide linkage between these residues. The evidence derives from solid-state NMR static echo and $n = 2$ rotational resonance experiments which probe the orientation of the ^{13}C carbonyl chemical shift anisotropy (CSA) tensor of the peptide bond with respect to the dipolar tensor connecting the carbonyl carbon to the ^{13}C-labeled α-carbon on the succeeding residue.

Introduction

Alzheimer's disease (AD) is the most common of the amyloidoses, a class of diseases which is characterized by the gradual accumulation of proteinaceous aggregates in various tissues of the body.[1] The detailed molecular structure of this fibrous, insoluble, noncrystalline material (termed amyloid) remains an open question, although the antiparallel β-sheet model proposed for *Bombyx mori* silk[2] has (with slight modification to account for a cross-β alignment) been widely adopted as a structural model.[1,3] More precise and detailed structural information may provide insight into both how and why these aggregates form.

The primary constituent of the amyloid plaques characteristic of AD are a family of 39−43 residue β-amyloid proteins (Aβ), where the variation in length occurs at the C-terminal end.[4] The longer variants of Aβ, particularly Aβ1−42, have been identified as crucial elements in the rapid formation of the insoluble fibrils which constitute amyloid plaque.[5−8] The 9-residue C-terminal fragment of Aβ1−42 (labeled β34−42, with sequence LMVGGVVIA, see Figure 1) forms a structured aggregate which is classified as amyloid primarily on the basis of its morphological and solubility properties and the classic cross-β fiber diffraction pattern it displays.[9] We have adopted the aggregate formed by this C-terminal fragment of Aβ1−42 as a model of the Aβ-dominated amyloid plaques associated with AD.

The results of a series of internuclear ^{13}C−^{13}C distance measurements along the β34−42 peptide backbone (reported previously[10]) indicate that the backbone conformation differs considerably from the fully extended conformation of the classic β-sheet, possibly including an unusual *cis* amide bond in the peptide's central glycyl−glycyl region.[11] Isotope-edited FTIR spectra of β34−42, which suggest an antiparallel β-sheet conformation for most of the peptide backbone, also indicate a deviation from that conformation in the glycyl−glycyl region.[12]

The internuclear distance information we have reported for the β34−42 peptide aggregate was obtained using the solid-state nuclear magnetic resonance (NMR) technique of rotational resonance (R^2).[13−15] This and related solid-state NMR techniques[16] provide a method for examining the detailed molecular

[†] Francis Bitter Magnet Laboratory, Massachusetts Institute of Technology.
[‡] Department of Chemistry, Massachusetts Institute of Technology.
[⊥] Center for Neurologic Diseases, Brigham and Women's Hospital, and Harvard Medical School.
[§] Current address: Walter Reed Army Institute for Research, 9100 Brookville Road, Silver Spring, MD 20910.
[∥] Current address: Magnetic Resonance Department, Schlumberger-Doll Research Laboratory, 110 Schlumberger Drive, Sugarland, TX 77478.
[⊗] Abstract published in *Advance ACS Abstracts,* September 15, 1997.

(1) Glenner, G. G. *New Engl. J. Med.* **1980**, *302*, 1283−1292.
(2) Marsh, R. E.; Corey, R. B.; Pauling, L. *Biochim. Biophys. Acta* **1955**, *16*, 1−34.
(3) Eanes, E. D.; Glenner, G. G. *J. Histochem. Cytochem.* **1968**, *16*, 673−677.
(4) Selkoe, D. *J. NIH Res.* **1995**, *7*, 57−64.
(5) Jarrett, J. T.; Berger, E. P.; Lansbury, P. T., Jr. *Biochemistry* **1993**, *32*, 4693−4696.
(6) Schneuner, D.; et al. *Nature Med.* **1996**, *2*, 864−870.
(7) Suzuki, N.; et al. *Science* **1994**, *264*, 1336−1340.
(8) Borchelt, D. R.; et al. *Neuron* **1996**, *17*, 1005−1013.
(9) Halverson, K.; Fraser, P. E.; Kirschner, D. A.; Lansbury, P. T. J. *Biochemistry* **1990**, *29*, 2639−2644.
(10) Lansbury, P. T. J.; Costa, P. R.; Griffiths, J. M.; Simon, E. J.; Auger, M.; Halverson, K. J.; Kocisko, D. A.; Hendsch, Z. S.; Ashburn, T. T.; Spencer, R. G. S.; Tidor, B.; Griffin, R. G. *Nat. Struct. Biol.* **1995**, *2*, 990−998.
(11) Spencer, R. G. S.; Halverson, K. H.; Auger, M.; McDermott, A.; Griffin, R. G.; Lansbury, P. T. J. *Biochemistry* **1991**, *30*, 10382.
(12) Halverson, K. J.; Sucholeiki, I.; Ashburn, T. T.; Lansbury, P. T., Jr. *J. Am. Chem. Soc.* **1991**, *113*, 6701.
(13) Andrew, E. R.; Bradbury, A.; Eades, R. G. *Nature* **1958**, *182*, 1659.
(14) Lowe, I. J. *Phys. Rev. Lett.* **1959**, *2*, 285.
(15) Raleigh, D. P.; Levitt, M. H.; Griffin, R. G. *Chem. Phys. Lett.* **1988**, *146*, 71−76.

S0002-7863(97)01494-7 CCC: $14.00

Aβ1-42: H_2N-DAEFRHDSGYEVHHQKLVFFAEDVGSNKGAIIGLMVGGVVIA-CO_2H

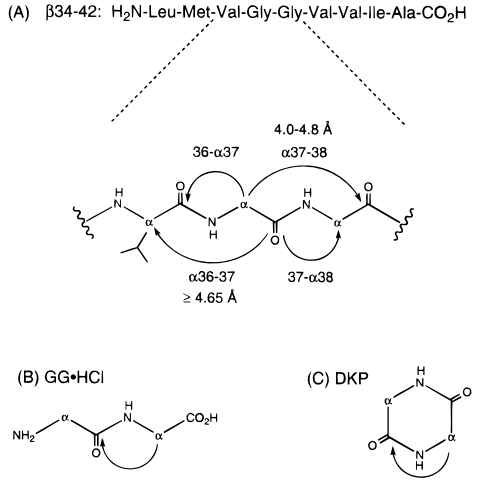

Figure 1. Aβ1−42 and β34−42 sequences and ^{13}C labeling schemes. (A) Central segment of β34−42 showing the four relevant $^{13}C_2$ labeling schemes. The α37−38 $n = 1$ R^2 distance measurement leaves in doubt the configuration of the 37−38 peptide bond, while the detailed examination of 37−α38 described here demonstrates a *trans* configuration. The α36−37 distance measurement reported previously indicates that the 36−37 peptide bond is *trans*, so that the 36−α37 sample serves as a control for the experiments described here. (B) 1−α2 labeling scheme in glycylglycine•HCl (GG•HCl), and (C) in diketopiperazine (DKP).

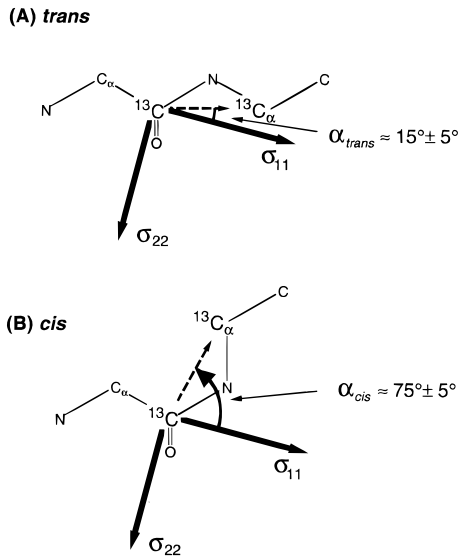

Figure 2. Diagram of carbonyl carbon CSA (solid vectors) and 1−α2 dipolar (dotted vector) tensor orientation as a function of peptide configuration. The carbonyl CSA tensor axes σ_{11} and σ_{22} point as indicated; the σ_{33} axis (not shown) is perpendicular to the page. The dipolar axis (dotted vectors) points along the internuclear vector.

structure of solid-phase material lacking the long-range order necessary to apply single-crystal X-ray diffraction techniques. Measurements of $^{13}C-^{13}C$ distances of up to 5−6 Å are feasible using the R^2 technique,[17,18] and the results of a series of measurements can be combined to examine structural features on a larger scale.

Synthesis of a series of $^{13}C_2$-labeled peptides, followed by processing of each to form ordered amyloid aggregates, provides samples in which the embedded ^{13}C nuclei are separated by distances that depend upon both peptide conformation (intramolecular distances) and packing (intermolecular distances) within the aggregate. Dilution of $^{13}C_2$-labeled material with unlabeled (natural abundance) material before aggregation reduces the number of intermolecular $^{13}C-^{13}C$ dipolar interactions, so that the intramolecular interaction can be studied in isolation. R^2 experiments are then performed by spinning the samples about the magic angle (thereby increasing spectral resolution) at a frequency that matches the isotropic chemical shift difference between the labeled ^{13}C nuclei (thus satisfying the $n = 1$ R^2 condition: $\delta = n\omega_r$, where δ is the isotropic chemical shift difference, ω_r is the sample spinning speed, and n is a small integer representing the order of the resonance). Matching the spinning speed to the appropriate R^2 condition in this manner avoids attenuation of the selected $^{13}C-^{13}C$ dipolar interaction which occurs at other spinning speeds.

The resonance effect is exploited to measure internuclear $^{13}C-^{13}C$ distances by creating longitudinal difference polarization and following its time-dependent decay due to $^{13}C-^{13}C$ dipolar evolution. Detailed analysis of the "magnetization exchange trajectory" obtained in this manner from dilute samples in which intermolecular effects are sufficiently attenuated allows (in principle) extraction of the intramolecular, internuclear distance because of the strong dependence of the decay rate on the dipolar coupling strength, and through it the internuclear distance. However for weakly coupled spin pairs corresponding to ^{13}C nuclei separated by 4−6 Å, the magnetization exchange trajectory is damped by zero-quantum (ZQ) line shape effects which must be accurately quantified to allow accurate extraction of the distance[10] (note that new R^2 techniques have been introduced which eliminate this problem[19,20]).

Uncertainty in estimates of the relevant ZQ line shape parameters and the possibility of residual intermolecular effects made it difficult to extract an accurate internuclear distance from exchange curves obtained from a β34−42 sample with ^{13}C labels at the α-carbon of Gly(37) and the carbonyl of Gly(38) (compound denoted α37−38, see Figure 1A). Initial experiments performed on undilute and 1:5 (labeled:unlabeled) dilute material did not detect a change in magnetization exchange rate with dilution (indicating no intermolecular interaction even in the undilute sample), and the 4.0 Å distance extracted from the data was interpreted to imply the possibility of a *cis* configuration at the glycyl−glycyl peptide linkage[11] (distances of under 4.2 Å between α- and carbonyl carbons on succeeding residues require either a *cis* configuration at the intervening peptide bond or a severely distorted *trans* configuration). The development of a new data analysis protocol that explicitly includes the effects of the inhomogeneous ZQ line shape[10] yielded a longer distance, on the order of 4.2−4.5 Å. Repetition of the initial experiment reproduced the original data in the 1:5 dilute sample but uncovered a strong dilution effect (a significantly faster exchange rate was observed in the undilute sample).[10] The proposed packing of the peptide within the aggregate has the glycyl−glycyl region of adjacent peptides in close proximity, so that a dilution effect of this magnitude is not unexpected. Furthermore, the size of the measured dilution effect suggests that, even at a 1:5 dilution, intermolecular contributions to the observed magnetization exchange rate are not fully attenuated, making the 4.2-4.5 Å distance a lower bound. Preliminary results of a measurement made on 1:10 diluted material which

(16) Bennett, A. E.; Griffin, R. G.; Vega, S. In *NMR Basic Principles and Progress*; Diehl, P., Fluck, E., Gunther, H., Kosfeld, R., Seelig, J., Eds.; Springer-Verlag: Berlin, 1994; Vol. 33, pp 1−77.
(17) Levitt, M. H.; Raleigh, D. P.; Creuzet, F.; Griffin, R. G. *J. Chem. Phys.* **1990**, *92*, 6347−6364.
(18) Raleigh, D. P.; Creuzet, F.; Das Gupta, S. K.; Levitt, M. H.; Griffin, R. G. *J. Am. Chem. Soc.* **1989**, *111*, 4502−4503.
(19) Costa, P. R.; Sun, B. Q.; Griffin, R. G. *J. Am. Chem. Soc.*, in press.
(20) Costa, P. R.; Sun, B. Q.; Griffin, R. G., manuscript in preparation.

indicate further attenuation of intermolecular effects are discussed below.

Although the 4.2−4.5 Å lower bound makes a *cis* configuration unlikely, the uncertainty raised by earlier experiments, together with the fact that much of the analysis just described was not made until the latter stages of our efforts, led us to develop solid-state NMR experiments to directly examine peptide bond configuration. Relative tensor orientation measurements, which have a long history in solid-state NMR, provide a means to extract structural parameters which are an alternative to internuclear distance measurements. The experiments presented here correlate the orientation of the chemical shift anisotropy (CSA) tensor associated with the carbonyl carbon in the peptide bond with the dipolar vector connecting the carbonyl carbon to the α-carbon on the succeeding residue. This requires a "1-α2" ^{13}C labeling scheme, where 1 indicates the ^{13}C carbonyl-labeled residue and α2 indicates the succeeding ^{13}C α-carbon-labeled residue. Experiments on appropriately $^{13}C_2$-labeled model *trans* and *cis* compounds (glycylglycine·HCl (Figure 1B) and diketopiperazine (Figure 1C), respectively) demonstrate that both static echo and $n = 2$ R^2 experiments can distinguish between the two configurations. Application of the techniques to 36−α37-labeled *β*34−42 confirms their reliability in amyloid material (the peptide bond between residues 36 and 37 in *β*34−42 is known to be *trans* from a previously reported α36−37 distance measurement[10] (see Figure 1A)). Finally, these techniques applied to 37−α38-labeled *β*34−42 clearly indicate a *trans* configuration at the peptide bond in question.

Experimental Section

$^{13}C_2$-Labeled Peptide Synthesis. [1-^{13}C]glycyl[2-^{13}C]glycine (labeling scheme denoted 1−α2 where 1 represents the *N*-terminal ^{13}C carbonyl-labeled residue and α2 represents the C-terminal ^{13}C α-carbon-labeled residue) was synthesized as follows. [2-^{13}C](*tert*-butoxycarbonyl)glycine was synthesized from the labeled glycine precursor (obtained from Cambridge Isotope Labs (CIL), Cambridge, MA) following standard procedures.[21] This compound was then coupled to the Kaiser oxime resin using standard protocols[9] to afford a substitution level of approximately 0.4 mmol/g resin. After standard deprotection and neutralization, tBoc−Gly (1-^{13}C) was coupled as the hydroxysuccinimide ester in methylene chloride using standard procedures. The product was cleaved from the resin using *N*-hydroxysuccinimide, and the resultant ester was reductively cleaved using zinc in acetic acid.[9] The tBoc protecting group was removed by treatment with trifluoroacetic acid in methylene chloride. The product was purified by HPLC and crystallized as the HCl salt (GG·HCl) according to published conditions.[22]

The first steps of the (1−α2)-labeled glycylglycine diketopiperazine synthesis were identical to those for glycylglycine described above. The oxime resin-bound, tBoc-protected dipeptide was deprotected with trifluoroacetic acid in methylene chloride (24 h at 25 °C) to remove the tBoc protecting group, and it was then treated with 5% diisopropylethylamine in methylene chloride to catalyze cyclization off the resin.[23] The product diketopiperazine (DKP) was purified by HPLC and crystallized from water according to published conditions.[24]

(36−α37)- and (37−α38)-labeled *β*34−42 peptides were synthesized using fluorenylmethoxycarbonyl (Fmoc) chemistry. Fmoc−Ala (residue 42) was shaken with 0.5 equiv of Wang resin in dimethylformamide containing 1.5 equiv of pyridine and 1.0 equiv of 2,6-dichlorobenzoyl chloride for 20 h. The derivatized resin was washed with methylene chloride and shaken with 3.5 equiv of benzoyl chloride and 6.3 equiv of pyridine in dichloroethane for 2 h.[25] Fmoc-protected amino acids were coupled sequentially using a standard method[26] (^{13}C-labeled Fmoc−amino acids were synthesized from ^{13}C-labeled precursor amino acids obtained from CIL). The resin-bound peptide was deprotected with piperidine in dimethylformamide and cleaved from the resin using 5% thioanisole in trifluoroacetic acid. The product was purified and characterized according to published procedures.[9]

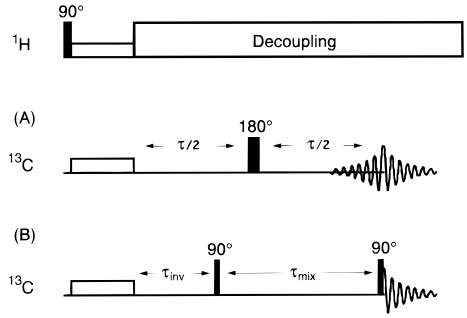

Figure 3. Pulse sequences for (A) static echo and (B) R^2 longitudinal mixing experiments.

All samples were 100% labeled, i.e., not diluted in natural abundance. The intermolecular contributions to the spin dynamics which dilution would attenuate are expected to be small, given the size of the intramolecular coupling (∼500 Hz) relative to typical intermolecular couplings (≤100 Hz). Supporting this assumption is the fact that 3-spin calculations for the GG·HCl sample which include the effects of the closest ^{13}C-labeled intermolecular spin to the intramolecular spin pair of interest show little difference from 2-spin calculations which do not include intermolecular effects (results of these calculations are not shown).

General ^{13}C NMR Methods. Experiments were performed either at 7.4 T (79.9 MHz for ^{13}C) or 9.4 T (100.0 MHz for ^{13}C) using custom-designed spectrometers and data acquisition and processing software courtesy of D. Ruben. Custom-built double-resonance probes of conventional design were outfitted with either 5 mm (spinning experiments) or 7 mm (static experiments) Doty (Columbia, SC) spinning assemblies. For the static experiments, the rotor was immobilized within the spinning assembly, and the spinning gas was turned on to allow for cooling to low temperature where necessary (described below). For the spinning experiments, the spinning speed was maintained within ±2 Hz of the set value with a Doty spinning speed controller. Both static and spinning experiments were performed with recycle delays of 1−3 s (this is substantially shorter than the ^{1}H T_1 in DKP; however, experiments with longer recycle delays of up to 1 min yielded identical results).

Static Echo Experiments. An echo sequence (Figure 3A) was used in the static experiments to differentiate between *cis* and *trans* configurations. After cross polarization[27] (CP) from ^{1}H to ^{13}C (typical rf field strengths 30−40 kHz; 2 ms duration), the ^{13}C magnetization is allowed to evolve in the transverse plane for a period $\tau/2$. A 180° pulse is applied on the ^{13}C channel, a second $\tau/2$ evolution period ensues, and the resulting echo is then detected**.** High-power CW ^{1}H decoupling (with a field strength of 80 kHz) is applied throughout the experiment after CP. Typically, 1000−5000 shots were acquired, and FIDs were processed with 0.5−0.75 kHz of exponential line broadening.

R^2 Experiments. A longitudinal mixing sequence (Figure 3B) was used in spinning experiments to detect the enhanced rate of magnetization exchange between coupled sites at the $n = 1, 2$ rotational resonance conditions (i.e., with the sample spinning speed set equal to, or half of, the isotropic chemical shift difference).[15] After CP (parameters similar to those listed above), a short period of transverse evolution occurs to create transverse difference polarization. Although best applied at high spinning speeds where side bands are absent from the spectrum, this inversion technique remained effective in the $n = 2$ R^2 experiments described here. A 90° pulse is then applied to create

(21) Itoh, M.; Hagiwara, D.; Kamiya, T. *Tetrahedron. Lett.* **1975**, 4393−4397.
(22) Koetzle, T. F.; Hamilton, W. *Acta Crystallogr., Sect. B: Struct. Sci.* **1972**, *b28*, 2083.
(23) Anderson, T.; Hellgeth, J.; Lansbury, P. T. J. *J. Am. Chem. Soc.* **1996**, *118*, 6540−6546.
(24) Degeilh, R.; Marsh, R. E. *Acta Crystallogr.* **1959**, *12*, 1007−1014.
(25) Sieber, P.*; Tetrahedron. Lett.* **1987**, *28*, 6147−6150.
(26) Sigler, G.; Fuller, W. D.; Chaturvedi, N. C.; Goodman, M.; Verlander, M. *Biopolymers* **1983**, *22*, 2157−2162.
(27) Pines, A.; Gibby, M. S.; Waugh, J. S. *J. Chem. Phys.* **1973**, *59*, 569−590.

Table 1. $^{13}C_\alpha-^{13}C{=}O$ Isotropic Chemical Shift Differences (Δ) and Carbonyl CSA Parameters (in ppm, Relative to Glycine ^{13}C Carboxyl at 177 ppm)

compound	Δ	σ_{11}	σ_{22}	σ_{33}
GG·HCl	127.38	245	176	87
DKP	124.29	242	185	80
37−α38	125.18	240	172	98
36−α37	129.29	243	180	95

longitudinal difference polarization, and dipolar mixing ensues. After mixing, a second 90° pulse is applied and the resulting FID is detected. Again, ^1H decoupling is applied throughout the experiment after CP (with a typical field strength of 80 kHz). The decay of longitudinal difference polarization as a function of mixing time is measured by repeating the experiment at a series of mixing times spanning the desired range. Residual difference polarization is calculated at each time point from integrated peak intensities, followed by a natural abundance subtraction on the order of 5−10% of the overall intensity.

Spin System Parameters and Dynamics Calculations. The relevant spin dynamics for both static and spinning experiments were calculated by numerical integration of the equations of motion derived from the rotating frame Hamiltonian,[28] interleaved with relaxation. Time steps were 1−3 μs. Powder averages included 500−1000 randomly selected crystallite orientations.

The relevant spin system parameters for the simulations were measured as follows. CSA tensor components were extracted from sideband patterns in slow-spinning spectra.[29] The resulting α-carbon tensors in all four 1−α2-labeled compounds can be roughly characterized by the parameters $\delta = -19.9$ ppm and $\eta = 1.0$. The isotropic chemical shift differences (Δ) and carbonyl CSA tensor components for the four compounds are listed in Table 1. The $^{13}C-^{13}C$ dipolar coupling constant for the 1−α2-labeled scheme is fixed by molecular geometry and was assumed to be 500 ± 10 Hz. The 1−α2 dipolar to carbonyl CSA tensor orientation is described by the Euler angles (0°, −90°, α°). For R^2 experiments, homogeneous and inhomogeneous ZQ line shape parameters were determined from single π-pulse Hahn echo experiments well away from rotational resonance using published methods.[10] Note that the large size of the coupling in these experiments makes the dynamics relatively insensitive to ZQ line shape parameters, as compared to the more weakly coupled spin pairs which have been examined extensively in amyloid to extract numerous distance constraints.

Background

Relative Tensor Orientation. The relative orientation of the carbonyl carbon CSA and carbonyl to α-carbon dipolar tensors in 1−α2 $^{13}C_2$-labeled peptides, as a function of peptide bond configuration, is shown in Figure 2. The carbonyl carbon CSA tensor is asymmetric and requires three axes to characterize its spatial dependence. The orientation of this tensor in glycylglycine·HCl (GG·HCl) has been measured directly from single-crystal NMR experiments[30] (combined with the neutron diffraction-derived crystal structure[22]) and serves as the model for carbonyl carbon CSA tensor orientation: the σ_{11} and σ_{22} axes are directed as indicated in Figure 2 relative to the molecular backbone, and σ_{33} (not shown) points into the page. The dipolar tensor is symmetric and can be represented as a single vector connecting the coupled atoms. For a *trans* configuration, the dipolar vector lies closest to the σ_{11} carbonyl carbon CSA axis, while for a *cis* configuration it approaches the σ_{22} direction. In both cases, the dipolar vector is expected to lie within 1−2° of the plane formed by σ_{11} and σ_{22}, so that we can adequately describe the relative tensor orientation by the single angle α between the σ_{11} axis of the carbonyl carbon CSA tensor and the dipolar vector. Static powder experiments in a series of G−X dipeptides[31] indicate a range for α in the *trans* configuration of 10°, with the value measured for the GG·HCl sample (19°) near one extreme ($\alpha_{trans} = 15 \pm 5°$). Other ^{13}C carbonyl carbon CSA tensor orientation measurements roughly agree with this range.[32−34] Calculating the value of α for the *cis* configuration by a 180° rotation about the peptide bond yields the value $\alpha_{cis} = 75 \pm 5°$.

Static Echo Experiments. The 180° pulse in the center of the echo period serves to refocus ^{13}C spin evolution due to chemical shift and heteronuclear dipolar couplings (particularly to ^{14}N, although this is only effective given a long enough ^{14}N T_1[35,36]). The remaining interaction of significance during this period in 1−α2 labeled peptides is the $^{13}C-^{13}C$ dipolar coupling, which drives oscillation of ^{13}C polarization between detectable single-quantum and undetectable antiphase states at a rate determined by the magnitude of the coupling. Because the strength of the dipolar coupling between spins depends on the orientation of the dipolar vector relative to the magnetic field, in powder samples (which by definition have an isotropic distribution of orientations) detectable single-quantum polarization will evolve to the undetectable antiphase state at different rates in different spin pairs. When the acquired signal is processed after a substantial echo period, we observe varying amounts of signal loss across the broad static spectrum in a pattern that depends upon the relative orientation of the dipolar and CSA tensors. Note that the correlation of chemical shift and dipolar tensors has been described previously,[37] and static dipolar-chemical shift experiments analogous to those described here have been used particularly to extract structural information regarding directly-bonded $^{13}C-^1H$[38] and $^{15}N-^1H$[39] spins.

Powder patterns calculated for the carbonyl carbon in 1−α2-labeled peptides as a function of relative tensor orientation α are shown in Figure 4. The solid lines indicate the powder spectra obtained with a very short echo period of $\tau = 50$ μs. This matches the shortest experimental mixing times (see below). A mixing period of this length is short enough to preclude significant dipolar evolution while still canceling the transient pulse effects that are often observed experimentally. The gray lines indicate the difference between that spectrum and the one obtained with $\tau = 750$ μs. The variation in the difference spectrum obtained after a substantial echo period as a function of relative tensor orientation α is clearly sufficient to distinguish between *cis* and *trans* configurations. (Small (<30°) deviations from amide planarity (simulations not shown) do not strongly affect the calculations.)

Rotational Resonance. At spinning speeds much larger than the relevant CSA magnitudes (a condition which often holds at the $n = 1$ R^2 condition for α-carbon−carbonyl $^{13}C_2$-labeled peptides), magnetization exchange dynamics in two-spin systems at rotational resonance are primarily determined by the magnitude of the dipolar coupling constant and the nature of ZQ

(28) Abragam, A. *The Principles of Nuclear Magnetism*; Oxford University Press: Oxford, 1961.
(29) Herzfeld, J.; Berger, A. E. *J. Chem. Phys.* **1980**, *73*, 6021−6030.
(30) Stark, R. E.; Jelinski, L. W.; Ruben, D. J.; Torchia, D. A.; Griffin, R. G. *J. Magn. Reson.* **1983**, *55*, 266−273.
(31) Oas, T. G.; Hartzell, C. J.; McMahon, T. J.; Drobny, G. P.; Dahlquist, F. W. *J. Am. Chem. Soc.* **1987**, *109*, 5956−5962.
(32) Hartzell, C. J.; Pratum, T. K.; Drobny, G. *J. Am. Chem. Soc.* **1987**, *87*, 4324−4331.
(33) Separovic, F.; Smith, R.; Yannoni, C. S.; Cornell, B. A. *J. Am. Chem. Soc.* **1990**, *112*, 8324−8328.
(34) Teng, Q.; Iqbal, M.; Cross, T. A. *J. Am. Chem. Soc.* **1992**, *114*, 5312−5321.
(35) Sachleben, J. R.; Frydman, V.; Frydman, L. *J. Am. Chem. Soc.* **1996**, *119*, 9786−9787.
(36) Weliky, D. P.; Tycko, R. *J. Am. Chem. Soc.* **1996**, *118*, 8487−8488.
(37) Waugh, J. S. *Proc. Natl. Acad. Sci. U.S.A.* **1976**, *73*, 1394.
(38) Stoll, M. E.; Vega, A. J.; Vaughn, R. W. *J. Chem. Phys.* **1976**, *65*, 4093−4098.
(39) Munowitz, M.; Huang, T. H.; Griffin, R. G. *J. Chem. Phys.* **1987**, *86*, 4362−4368.

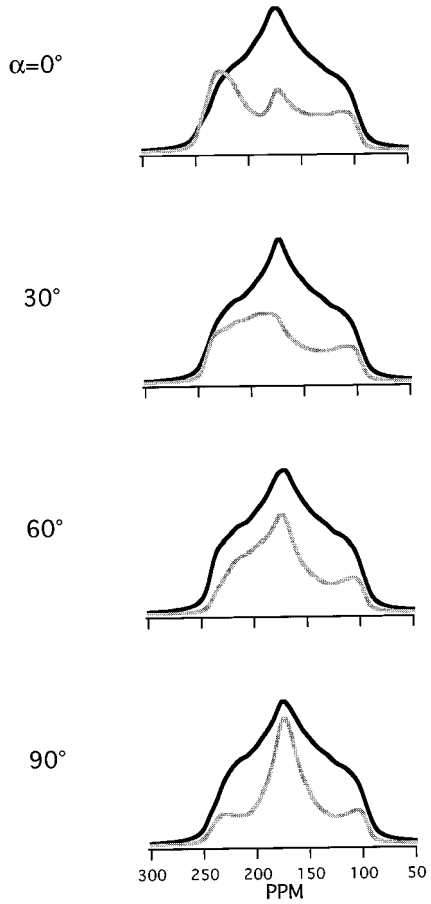

Figure 4. Calculated carbonyl static echo powder spectra for 1−α2-labeled peptides as a function of the relative tensor orientation angle α. Solid lines indicate the spectrum obtained with essentially no echo period ($\tau = 50$ μs); gray lines indicate the difference between that spectrum and the one obtained with $\tau = 750$ μs.

damping effects. The ZQ line shape parameters which are necessary to characterize the damping can be extracted from single π-pulse Hahn echo experiments away from resonance, so that the remaining unknown—the dipolar coupling constant (and hence the internuclear distance)—can be extracted with some accuracy from the R^2 exchange data.[10,20]

At spinning speeds which are not larger than the CSA magnitudes, there is additional dependence of the magnetization exchange dynamics on the relative orientation of the relevant CSA and dipolar tensors.[17,40] For α-carbon−carbonyl $^{13}C_2$-labeled peptides this typically occurs at the $n \geq 2$ R^2 conditions. Because the dipolar coupling constant in 1−α2-labeled peptides is approximately fixed (∼500 Hz) by molecular geometry, relative tensor orientation becomes the unknown variable which we can then attempt to extract in experiments of this type. Figure 5 shows the calculated variation in the magnetization exchange curves for an $n = 2$ experiment as a function of dipole-to-CSA orientation in an idealized 1−α2 system where the relatively small α-carbon CSA has been ignored. With the dipolar vector aligned along the σ_{11} axis, the slowest exchange rate is observed; along σ_{22}, an intermediate rate; and along σ_{33}, the fastest rate. The trend can be stated as follows: the magnetization exchange rate increases as the carbonyl CSA shielding along the axis defined by the dipolar vector increases. (A similar trend is seen in $\eta = 0$ tensors and can be explained by close analysis of largest two sideband products in the appropriate CSA and dipole convolution. It is interesting to note that for many orientations,

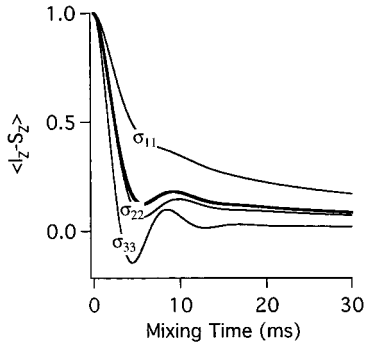

Figure 5. Calculated $n = 2$ R^2 exchange curves for 1−α2-labeled peptides as a function of relative tensor orientation. With the dipolar vector along the least-shielded carbonyl CSA σ_{11} axis, magnetization exchange is minimized; as it moves to the most-shielded σ_{33} axis, exchange is maximized. For comparison, the curve without CSA (thick line) is also displayed.

the presence of the CSA interaction increases the dipolar exchange rate because it folds in $m = 1, 2$ dipolar components. In the absence of relaxation effects, polarization transfer efficiencies exceeding 90% are possible given the appropriate orientation.) As illustrated in Figure 2, the *trans* and *cis* configurations have the dipolar vector approximately along the σ_{11} and σ_{22} CSA axes, respectively, and so have different magnetization exchange dynamics at the $n = 2$ R^2 condition that can be used to distinguish between the two orientations.

Results and Discussion

***n* = 1 R² Distance Measurements on α37−38.** Magnetization exchange curves obtained at the $n = 1$ R^2 condition for undilute and 1:5 (labeled:unlabeled) dilute α37−38 samples show very different exchange rates. The much accelerated rate of exchange obtained from the undilute sample presumably comes from intermolecular dipolar interactions due to packing, in addition to the single intramolecular interaction. This is supported by the proposed alignment of peptide monomers in the aggregate, which yields intermolecular interspin distances on the order of 4.5−5.5 Å for the α37−38 spin pair. Recent attempts to quantitatively simulate the data obtained from the 1:5 dilute sample, assuming only two interacting spins and using a series of interspin distances spanning the possible range, have been unsuccessful. The exchange rate at early times (<10−15 ms) is relatively rapid and suggests a distance in the 4.1−4.3 Å range, while the rate at later times (15−35 ms) is slower and suggests a distance of 4.4−4.6 Å.

The distortion in the shape of the exchange curve can arise from several causes, including inaccurate estimates of the relevant ZQ line shape parameters. Recent experiments in model and amyloid systems indicate that our methods for estimating these parameters are correct.[20,41] A more likely explanation is that the 1:5 dilution does not sufficiently eliminate intermolecular contributions to the exchange dynamics. Multispin simulations support this conclusion by showing a similar distortion of the exchange curve—an overall increase in the exchange rate at all times that is largest at early times. The size of the dilution effect on going from the undilute to the 1:5 dilute sample and the proximity of α37−38 spin pairs on adjacent β34−42 monomers in the proposed β-sheet[10] are also consistent with this explanation.

Preliminary experiments in a 1:10 diluted sample of β34−42 were performed in parallel with the tensor orientation experiments described here to ascertain whether significant

(40) Tomita, Y.; O'Connor, E. J.; McDermott, A. *J. Am. Chem. Soc.* **1994**, *116*, 8766−8771.

(41) Costa, P. R.; Sun, B. Q.; Kocisko, D. A.; Lansbury, P. T., Jr.; Griffin, R. G., unpublished results.

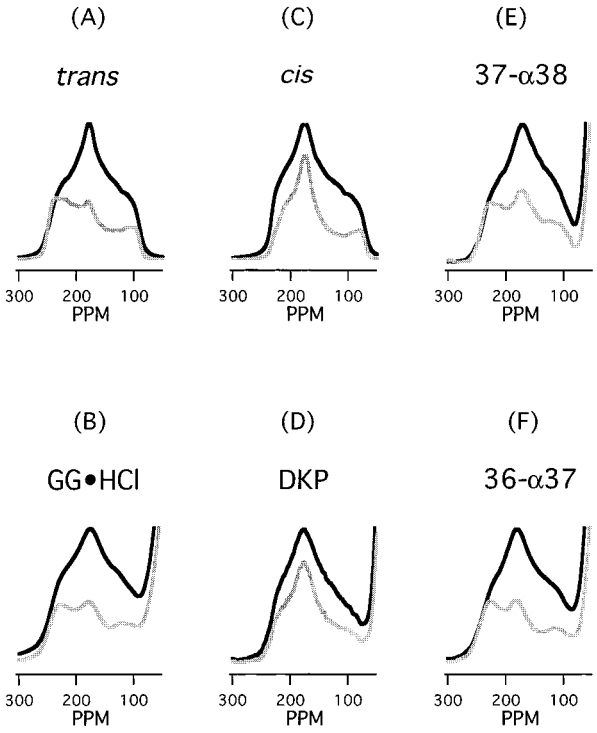

Figure 6. Calculated and experimental static echo powder spectra for 1−α2 labeled peptides. Solid lines indicate the $\tau = 50$ μs powder pattern; gray lines indicate the difference between that spectrum and the one obtained at $\tau = 750$ μs. (A) Calculated spectra for the *trans* configuration. (B) Experimental spectra for GG·HCl (the rising edge on the right side of the spectrum is the α-carbon peak). (C) Calculated spectra for the *cis* configuration (α = 65°). (D) Experimental data for DKP. (E) Low-temperature ($T = -110$ °C) experimental spectra for 37−α38-labeled β34−42. (F) Low-temperature (T = −170 °C) experimental spectra for 36−α37-labeled β34−42.

intermolecular couplings are present in this sample at a 1:5 dilution. The data indicate that a further reduction in the exchange rate has occurred, suggesting that the intramolecular distance is longer than our previous estimates. This experiment makes the existence of a *cis* amide highly unlikely.

Static Echo Experiments. Static echo experiments performed at room temperature on $^{13}C_2$-labeled GG·HCl and DKP (1-α2 labeling scheme) yield the results in parts B and C, respectively, of Figure 6. The solid lines in each plot indicate the powder spectrum obtained with essentially no dipolar mixing (a 50 μs echo period was used to avoid transient pulse effects), and the gray lines indicate the difference between that spectrum and the one obtained with a mixing time of 750 μs. Simulated curves for GG·HCl (Figure 6A) were calculated using the measured CSA tensor magnitudes, the estimated dipolar coupling constant, and the carbonyl CSA-to-dipolar tensor orientation calculated from the single-crystal experiment[30] (α = 19°).

For DKP, no single-crystal NMR study exists fixing the carbonyl carbon CSA tensor in the molecular frame. If one assumes that the *cis* configuration can be derived from the known *trans* configuration of glycylglycine solely by a 180° rotation about the peptide bond, then the expected dipolar-to-CSA orientation should be characterized by α ≈ 75°. A series of simulations about this value indicate that α = 65° (Figure 6D) provides a better fit; we therefore use this as the canonical *cis* value in what follows. The distortion of the carbonyl carbon CSA tensor orientation in DKP relative to that in GG·HCl that this implies is small and does not materially affect our ability to distinguish between *cis* and *trans* configurations using the techniques described here. That the distortion does not involve a large rotation (>30°) of the σ_{33} axis away from its assumed perpendicular direction with respect to the amide plane (defined here by the carbonyl C and O atoms and the amide N) was confirmed by comparison of the experimental data to additional simulations including this effect (not shown).

Identical experiments were applied to two $^{13}C_2$ β34−42 compounds, one with labels spanning the glycyl−glycyl peptide linkage in question (labeling scheme 37−α38) and, as a control, one with labels spanning the previous peptide linkage (36−α37), known to be *trans* based on previous R^2 distance measurements[10] (Figure 1). At room temperature, the difference spectra (not shown) showed excess intensity spanning all frequencies. This likely indicates the presence of ^{14}N relaxation[35,36] and/or small-scale molecular motion on a relatively short (0.1−1 ms) time scale.[42] Chemical exchange experiments[42] (results not shown) with mixing times spanning the range 0.1−30 ms indicate that what motion is present (if any) must occur on the 0.1−1 ms time scale mentioned and have small amplitude (too small to accurately quantify using these techniques, i.e., corresponding to a rotation of < 10−30° about some axis).

Experiments conducted at sufficiently low temperature will freeze out motion and increase the ^{14}N T_1, eliminating distortions arising from either effect. Repeating the experiments at low temperature yielded the results shown in Figure 6E for 37−α38 ($T = -110$ °C), and in Figure 6F for 36−α37 ($T = -170$ °C). In both cases the experimental data more closely match *trans* than *cis* simulations (Figures 6A and 6D, respectively). The slightly elevated central peak in the difference spectrum obtained for the 37−α38 compound at low temperature (Figure 6E) might indicate (i) a dipolar-to-CSA orientation closer to α = 30°, (ii) a combination of *cis* and *trans* patterns due to the presence of both configurations in the amyloid fibril, or (iii) a temperature that is not sufficiently low to fully eliminate the distortions observed at room temperature. Close examination of the experimentally obtained powder pattern (Figure 6E) indicates that the first explanation is incorrect since the overall shape of this difference spectrum does not match that expected for α approaching 30° (see Figure 4). The second explanation would require that multiple conformations also be present at room temperature, although motion between them that is not evident at low temperature might occur at this higher temperature. The absence of line shape distortions (splittings, etc.) in the room-temperature high-resolution (MAS) chemical shift spectra of ^{13}C nuclei all along the peptide backbone[10] makes it unlikely that more than one motionally averaged conformation is present in detectable amounts at room temperature. The absence of significant motion at room temperature (such as that necessary to move between *cis* and *trans* configurations) is demonstrated both by the chemical exchange experiments described above and by the fact that the room-temperature carbonyl CSA tensor magnitudes closely match those obtained at low temperature. The third explanation is the most likely—the temperature is not low enough to fully remove the distortions present at room temperature.

***n* = 2 R^2 Relative Tensor Orientation Measurements.** Longitudinal exchange experiments at the $n = 2$ R^2 condition were made in each of the four (1−α2) $^{13}C_2$-labeled samples—GG·HCl and DKP as *trans* and *cis* models, respectively, and 36−α37- and 37−α38-labeled β34−42. The experimental exchange curves (open circles) are shown in Figure 7A−D, along with simulated exchange curves for both *trans* (α = 19°; solid lines) and *cis* (α = 65°; dotted lines)

(42) Schmidt-Rohr, K.; Spiess, H. W. *Multidimensional Solid State NMR and Polymers*; Academic Press: London, 1994.

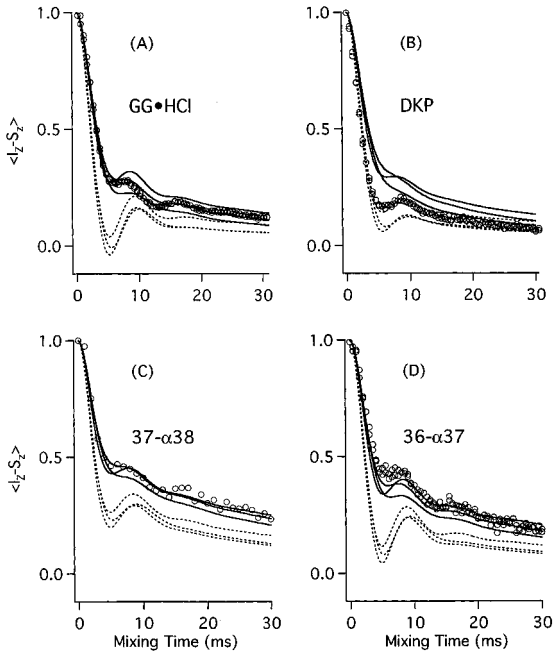

Figure 7. Calculated and experimental $n = 2$ R^2 exchange curves for 1−α2-labeled peptides. Open circles indicate experimental data; solid lines indicate *trans* simulations; dotted lines indicate *cis* simulations. (A) GG·HCl; (B) DKP; (C) 37−α38-labeled β34−42; (D) 36−α37-labeled β34−42.

configurations. The set of three simulations for each configuration takes into account the unknown orientation of the α-carbon tensor, indicating the expected results for three extreme orientations of that tensor. Comparison of experimental data to simulation suggests a *cis* configuration for the DKP sample and *trans* for the others. This is in agreement with the results from the static echo experiments.

Conclusion

Previous measurement of the distance between the 37 α- and 38 carbonyl carbons along the β34−42 peptide backbone yielded an anomalously short value (4.0 Å) that was interpreted to imply either a *cis* or a severely distorted *trans* configuration at the intervening peptide bond.[11] Subsequent modification of the R^2 simulation technique and the observation of strong intermolecular interactions in this sample indicated that a longer internuclear distance was likely. The experiments detailed here demonstrate that the peptide bond between residues 37 and 38 is in the *trans* configuration.

This eliminates from the proposed family of β34−42 structures[10] those with a glycyl−glycyl *cis* peptide bond (15 of 178 structures). The remaining structures are all characterized by two regions of highly pleated β-strand structure flanking the central glycyl−glycine sequence. ^{13}C isotope-edited FTIR data[12] and peptide aggregation experiments on amide-to-ester variants of β34−42[43] continue to suggest unusual structure in this central region, which may be critical for intermolecular packing.

Acknowledgment. This work was supported by grants from the National Institutes of Health (GM-23403, NS-33366, RR-00995).

JA971494B

(43) May, C.; Weinreb, P. H.; McGuinness, B.; Lansbury, P. T., unpublished results.